Back to Session Subjects

PITCH-UP PHENOMENON CHARACTERIZATION BY MEANS OF HW AND PIV MEASUREMENT TECHNIQUES

D. Barbagallo, F. De Gregorio, N. Tino

CIRA – Italian Aerospace Research Centre

Abstract

An experimental campaign was performed in the 24ft open jet subsonic Wind Tunnel at DERA-Farnborough Research Centre in the framework of the Brite-Euram project named "HELIFLOW". The project objective was to improve experimental and theoretical tools for helicopter aeromechanics and aeroacustic interactions. The present work describes the experimental investigation performed by means of Particle Image Velocimetry (PIV) and Hot Wire Anemometer (HWA) techniques to qualify (investigate) the rotor wake behind a 1:2 scaled helicopter model in forward flight at different advance ratio values (μ= 0.015÷0.05) at c_T/σ=0.08 thrust level and at α_S=2° shaft angle.

The present research work will address effects due to low speed interference named "pitch-up", during transition from hover to forward speed. The phenomenon results from the changes of the pitching moment associated with the main rotor wake impinging on the rear of the fuselage, tailplane and tail rotor of the helicopter.

Quantitative measurements of flow field have been performed, resulting in a map of the flow in the zone of the tailplane (TP) with a clear individuation of tip vortex, velocities behaviour, frequency characteristics, flow status on the tailplane and rear fuselage. A comparison of the results obtained with the two techniques will be showed. This measurements have also detected the position of the rotor wake impinging on the tailplanes and it will be compared with results of the previous tests performed to measure the force acting on the tail planes in order to detect the advance ratio at which the tail planes were effected by rotor downwash.

Nomenclature

σ: Rotor solidity

CIRA : Italian Aerospace Research Centre

c_T: Non dimensional thrust coefficient

DERA : Defence Evaluation and Research Agency

FFT: Fast Fourier Transform

HWA : Hot Wire Anemometer

Kt: Tangential Sensitivity Coefficient

PIV : Particle Image Velocimetry

TP: Tail plane

U,V_x: Axial Flow Velocity Component

Ueff: Effective Velocity

Vy: Transverse Velocity

W,Vz: Vertical Flow Velocity Component

α_S: Shaft angle

μ: Advance Ratio

1. Introduction

The development of analytical methods to predict a rotor performance are increasing in accuracy. Nevertheless, none of these is self-contained; they all require the characteristics of the wake in order to have correct downwash distribution. The rotor data can be obtained by surface pressure transducer [1, 2]. In the past the rotor wake geometry has been investigated by means of flow visualisation techniques [3-5] and by LDV [6-8]. A detailed investigation of the wake flow structure has been made by means of HW technique [9-11].

Anyway, in spite of the growing capacity of analytical models, the development of new helicopters is impossible without time-consuming and expensive test. The more complex aerodynamics and structural dynamics of rotorcraft specifically require adequate tests addressing such effects as interference between rotors and fuselage components and the coupling between aerodynamic and aeroelastic characteristics.

Since the maturity of theoretical model is not yet satisfactory, experimental approaches are mandatory.

The present research work will address effect due to low speed interference named “pitch-up”, during transition from hover to faster forward speed. The aerodynamic interactions between the rotor wake and the tailplanes of the helicopter are known to be particularly complicated [12]. Resolving this problem can require substantial tail redesign and significant flight testing time. The difficulties with the horizontal tailplane design on he AH-64 Apache and EH-101 helicopters are documented examples [13].

While there have been several reported rotor/airframe interaction studies with essentially non lifting fuselage shapes systematic experimental studies involving lifting components are rare. Due to the importance of the phenomenon and the lack of the detailed experimental data, the European Commission has supported a dedicated study on Pitch-Up using both numerical and experimental simulations in the framework of the BRITE/EURAM project named “HELIFLOW”. The present work will report only the results of the measurement campaign performed by means of Particle Image Velocimetry (PIV) and Hot Wire Anemometer (HWA) systems to investigate the flow field characteristics near the tail plane positions. The objectives of the experimental research are to:

- demonstrate the reliability of the HWA and PIV measurement techniques on complex unsteady flow in a industrial facility
- investigate the flow conditions resulting from the changes of aircraft pitching moment associated with the main rotor wake impinging on the rear of the fuselage and tailplanes
- compare the measurements with HWA and PIV systems
- provide accurate velocity field measurements in order to validate numerical codes.

2. Measurement Description

The measurements have been carried out on a 1:2 scaled helicopter model designed and provided by AGUSTA with main rotor diameter of 3 m (fig.1). The model allowed to mount the tail planes in five different positions, as shown in fig.2, in order to investigate the pitch up phenomenon for different model configurations.

In the “fig.2” is also shown the adopted reference system. The system is related to the wind tunnel. The system is defined as follows: the plane z=0 is a horizontal plane containing the trailing edge and the leading edge of the tail planes when the shaft angle position of the model is zero, the plane y=0 is a vertical plane containing the external line of the pressure transducers, positioned approximately at 83% of the tail plane spanwise, the plane x=0 is a vertical plane containing the leading edge of the tail plane in position 2.

The tail positions and the test conditions were selected by the analysis of the force acting on the tail planes measured during a much wider measurement campaign performed by DERA[14]. The lift, measured by the tail plane balances Vs advance ratio, showed that the most forward position of the tail plane (position 1) was affected by the main rotor wake for all the condition. Whereas the centre and aft tail positions (position 2 and 3) were influenced by the main rotor wake at advance ratio 0.015 and 0.03 respectively. On the base of these data the test matrix was chosen for the position 2 and 3 of the stabiliser. The test conditions are summarised in the following:

- 1 rotational speed of the rotor (1400 r.p.m)
- 2 tail positions (2, 3)
- 1 shaft angle position (+2°)
- 5 advance ratio (0.015, 0.02, 0.03, 0.04, 0.05).

Both PIV and HWA measurements have been carried out removing the tail plane by the fuselage. The instantaneous velocity fields have been investigated by means of PIV technique in correspondence of the tail position 2 and 3. For each tail position, the area above the tail plane and immediately in front of the leading edge have been measured as shown in “fig 3”. For the centre position of the tail plane two areas have been acquired. The zone, called A2, is located above the tail plane and it is delimited by the following co-ordinate –18.3mm<x<162.3mm, y=0 and -8.5mm<z<135.9mm, and the zone, called B2, positioned in front the tail plane leading edge (delimited by the following co-ordinate: –165mm<x<15.5mm, y=0, –51.4mm< z <93mm).

For the aft position of the tail plane two areas have been acquired. The zone, indicated as A3, is located above the tail plane (delimited by the following co-ordinate: 191.3mm<x<371.7mm ,y=0 and 4.1mm<z<148.5mm) and the zone, called B3, positioned in front the tail plane (delimited by the following co-ordinate –44.8mm<x<135.8mm, y=0 and –89.6mm<z<54.8mm). The zone B3 was located more forward of the tail plane position 3 in order to collect the boundary of the wake with relative tip vortex.

Following HWA measurements have been performed with a 2-D probe (X probe type) mounted on the DERA traversing system in order to validate the PIV results and to investigate the time history of the flow field. The traversing system was positioned adjacent to the rotor rig and parallel to the airstream. The measurements were recorded at the tail plane height

covering approximately the same distance as the PIV tests. The HWA measurements with X probe have regarded two different positions of the tail plane (removed) on both side of the model. The zone of the tail plane in line with the outboard pressure transducer station (long the x axis) has been investigated. For each condition, the traverse has covered the distance from the point 20 cm ahead of the tailplane leading edge to the trailing edge, i.e. overall 35 cm with an approximate step of 1 cm "Fig.4".

The HWA measurements with glue on probes have regarded the tail plane and the fuselage. Their location is described in the section regarding the glue on results.

3. Wind Tunnel Layout and Performed Modification

The DERA 24ft Wind Tunnel "Fig.5" has an open jet working section 24 feet (7.3 m) in diameter with a large plenum chamber; maximum speed is 50m/s although the use of safety netting reduces the maximum to 44m/s, 0.2 advance ratio. The lowest controllable speed of the wind tunnel without the rotor rig is 3m/s. The wind tunnel has all of the necessary fixed installations and fittings to enable installation of the Model Helicopter Rotor Test Rig [16].

The rotor test rig comprises a drive system, test tower, rotor hub and blade pitch control system, 6 component rotor and fuselage balances with fully computer controlled data acquisition and monitoring system. The motor drive control system provides 150 kW of power at the rotor shaft for a 3m diameter model rotor running at 1400 r.p.m.; rotor tip speed is 220 m/s. The rotor system used consisted of a four-bladed, fully articulated hub. The blade set, designated PM1, has a 0.12m chord, a linear –8deg twist over the 1.5 m radius and an advanced RAE9646 airfoil section. More details on the above topics are reported in [17].The fuselage has been designed, built and provided by AGUSTA.

In the fig.5, the locations of the seeding rake, the seeding generator and the acquisition digital camera are illustrated. In order to apply Particle Image Velocimetry technique, at 24ft wind tunnel, some preparation were undertaken by DERA in accordance to the requirements provided by CIRA. The PIV test technique requires vibration-free platforms for the laser equipment and video camera. A platform, large enough to accommodate all the required locations of the laser equipment, was designed and manufactured. The platform was installed above the existing flexible test section floor on a rigid framework that was in turn attached to the concrete floor and therefore isolated from vibrations coming from the rotor rig. A second stable platform was manufactured and installed for the PIV camera. The platform was positioned approximately 3 m above the test section floor and to the port side of the rotor rig. Following, this platform will be indicated also as balcony.

The HWA acquisition system was installed under the test chamber floor. During the HW tests a 1D traversing systems was installed adjacent to the rotor rig and parallel to airstream.

4. PIV Experimental Set Up

The tests were performed with the fuselage pressure-transducer panels replaced with blanks avoiding pollution or damage by seeding particle and the tail plane removed.

A Nd:YAG pulse laser was mounted on the platform prepared below the rotor rig in the test chamber. The whole laser system and the optical lens set up was built up on an optical bench using commercially available X-95 elements. This results in a stable but still very flexible and compact set up. The height of the laser system was minimised in order to avoid any disturb to the tunnel flow. The light sheet formed was 350 mm wide and 2-3 mm thick. The laser was located at approximately 5 m below the area of interest "Fig. 6".

The flow field of the rotor slipstream presents a strong 3D behaviour. Due to this the number of the out of plane particles increase while the signal/noise ratio decreases. To avoid this a larger thickness of the light sheet (2-3mm) and a shorter delay time between the light pulses (10 μs) have been used. The digital camera has been positioned above the apposite balcony, fixed to a frame built by means of X95 optical bench. The camera is a full frames interline CCD technology, it allows to acquire two frames with minimum delay of 1 μs and a CCD resolution of 1024 by 1280 pixels. In order to reduce the black current, the CCD is cooled by a Peltier cell. The light intensity is stored on 12 bit instead of the classical 8 bit, increasing the dynamic range of the measurement and doubling the dimension of the image files. Calibration was done with a reference grid inserted in the test section at the position of the light. The calibration grid was mounted on the support of the tail plane sheet as shown in "Fig.6". The instantaneous velocity fields, dimension about 18x15cm^2 , have been acquired, by the digital camera, from a distance up to 7 m, using a 300mm lens with f-number of 2.8. The lens has been equipped with a home made control focusing system in order to adjust the image sharpness from remote position.

To insert homogeneously the seeding particles in the tunnel, a seeding rake has been positioned at the exit of the nozzle. The rake is able to seed an area of about 2.3x0.8 m^2 . The rake has been fed with two of the CIRA particle generators which also have been

positioned in the test chamber providing atomized olive oil particles of 1µm mean diameter. For safety reason the complete acquisition system has been driven from the area located on the back of the tunnel control room where the PC was positioned. In this way the control unit was located approximately at 15 m from the digital camera and at a distance up to 20 m from the pulse laser.

5. HWA Experimental Set Up

The tests were performed in the same condition foreseen for the PIV tests, with the tail planes removed. The HWA measurements were performed with two types of probes:

- 2-D probe (called X probe)
- Glue-on probes (called surface-mounted probe).

The X probe is made of two cylindrical sensors oriented at 90° to each other. The X probe is used to measure two velocity components in the plane of the sensors. The third component is obviously neglected giving an estimated error of about 8% when the turbulence intensity is less then 20%[18- 19]. The X probe used during the tests was a TSI - Model 1241-20. Due to the industrial environment a 2D platinum Hot Film, 50.8 microns in diameter, about 1.02mm long was selected. The X probe provides two analogic signals related to velocity components in the sensors plane.

As surface-mounted hot-film, the DANTEC glue-on probes have been used. They consist of a nickel heating film (0.9 x 0.7 x 0.001mm^3) deposited on a polyamide foil (8 x 16 x 0.05 mm^3). The polyamide foil is glued directly onto the surface at the required measuring point. These probes are commonly used to investigate the status of the flow and to measure the mean wall shear stress (skin friction). The tests have regarded only the survey of the status of the flow.

The used anemometer was the TSI IFA 100, a constant temperature anemometer fit with four channels. The anemometer measures fluid velocity by sensing the changes in heat transfer from small, electrically-heated element exposed to the fluid. Being the heat transfer influenced by the air conditions (velocity, temperature and pressure), the probe calibrations have been performed at the beginning and at the end of each wind tunnel run. For the above purpose the low turbulence TSI calibration unit was installed at 24 ft DERA WT. This unit is provided of pressure transducer to monitor the velocity and probe rotator that allows angular calibrations for the X probe.

The IFA 100 output analog signal is sent to a personal computer that is provided with a MetraByte board (DAS-20) that converts the signal to digital voltage data and store them on the hard disk. The data acquisition board operates in 16-channels, single-ended or 8-channels, differential-input modes. Seven software-selectable input ranges are available including unipolar (e.g. 0 to 10V) and bipolar (-10 to +10V) configuration. A/D functions use a successive-approximation converter that performs just over 100.000 conversion per second. The acquired voltage data are analyzed by mean of dedicated software developed by CIRA. The acquisition chain is completed with an oscilloscope to monitor the signals and have a ready response to any problems during the tests.

To transverse the X probe in the zone of the measurements, DERA provided a 1D traversing system moved by an electrical step motor. The pylon with probe holder was about 5m high and was strengthen with 3 steal connecting rods in order to reduce the vibrations “Fig.7”. The traversing system was positioned on both side of the fuselage in order to investigate the wake behaviour before and after impacting on the fuselage.

6. Data Analysis

6.1. PIV

In the present work only part of the acquired data by means of the PIV system will be presented. The complete set of results have been presented elsewhere [20, 25].

About 740 image pairs, related to 17 different test conditions, have been acquired. For each test condition about 50 pairs of images have been taken in order to investigate the instantaneous flow structures and, averaging over all the instantaneous measurements, the mean flow field. The images have been evaluated by means of the cross-correlation method using interrogation windows of 32^2 pixels, the interrogation windows have been overlapped 50% providing a matrix of 79x63 displacement vectors. To improve the signal/noise ratio the multi pass algorithm has been used, in which a number of passes is used to shift the interrogation window with respect to each other in accordance with the local displacement vector. This procedure as described in Willert [21], has the advantage of significantly reducing the measurement uncertainty and improving the signal to noise ratio of the cross-correlation function (i.e. higher data yield). Between each of the interrogation passes an out-layer search algorithm eliminates vectors which significantly deviate from their neighbours to prevent the following interrogation iteration to lock onto the suspect displacement data. In the final pass, the peak detection algorithm is limited to a smaller search

region within the correlation plane to recover displacement data, which may not otherwise be found.

The spatial resolution of the vector matrix is less than 2.6 mm. Sequentially a filter algorithm to remove to outliers vectors and a filter pass to replace the hole with vectors evaluated from the average of the neighbours values have been applied. After that the displacement vector field is converted in the velocity field and the new origin of the reference system is calculated.

6.2. HWA

The Data Acquisition System for the tests with X probe was configured to acquire the signal for 1 second at a sample rate of 28320Hz. In 1 second the rotor performs about 23 complete rotation that is about 93 blade passages. All the data were acquired simultaneously to the trigger from the rotor rig that gave a square wave for each rotation. A total number of 346 different position have been acquired by means of X probe. The acquisition with X probe for each advance ratio condition foresaw about 35 steps of 1 cm each for an amount of 36 files containing the two voltage signal and the rotor rig trigger signal.

The stored data of each sensor have been converted in effective velocity by means the calibration curve. The calibration curve is obtained interpolating the calibration points by a best fit polynomial of the fifth order which has been verified [22], to give a standard deviation of order 0.1%[19]. To separate the velocity components (u, w), the so called squared effective velocity [19] has been used, resulting in a system of two equations in two unknowns as in the following:

$$\begin{cases} U_{eff\,1}^2 = K_{t1}^2 * X + Y \\ U_{eff\,2}^2 = K_{t2}^2 * Y + X \end{cases}$$

$$X = \left[u\left(\sqrt{2}/2\right) + w\left(\sqrt{2}/2\right) \right]^2$$

$$Y = \left[u\left(\sqrt{2}/2\right) - w\left(\sqrt{2}/2\right) \right]^2$$

and K_t [23] is the tangential sensitivity coefficient. The system is linear in variable X and Y and can be solved directly using Kramer method allowing the determination of the velocity components in the plane of the sensors.

For the tests with glue-on probes the sample rate was 19824 Hz for a period of two second. For each test 4 glue-on probes were monitored. A set of 4 glue-on probes were mounted on the fuselage and another set on the left tailplane. The glue on probes data will be presented in terms of voltage because no calibration is needed for knowing the status flow survey. Moreover the standard deviation has been evaluated.

In fact the glue on probes have the sensing element glued on the surface of the model. The HW System monitors the voltage level during the test. This level is then compared with the voltage when the velocity is null. This comparison gives the indication if the flow is attached or separated on the surface. In fact, if there is flow on the sensor, the resulting cooling effect that depends on the velocity derivative at the wall, causes an increase in the voltage supply by the HW System to keep the temperature constant. The calculation of the standard deviation can give information on the type of the flow, when attached.

7. X-probe HW Results

The aim of this section is to describe the results of the test performed with the 2-D probe in vicinity of the tail plains position number 2 and 3. The data where acquired simultaneously to the trigger from rotor rig that gave a square wave for each rotation. The velocities [15] clearly show that the phenomenon is obviously really periodic and the shape of the signals depends by the zone of investigation. The time histories have been analysed in different ways as in the following:

- The time history is averaged along all the time interval in order to have the mean value of the velocity for each spatial position
- The time history is splitted in each rotation and they all have been averaged to extract the behaviour of the flow within a complete rotation.
- The time histories have been analysed in terms of FFT to highlight the frequencies characteristics of the phenomenon.

7.1. Time-Averaged Velocity Field

As stated earlier, the velocities were measured in proximity of tail planes to document the general characteristics of the wake and to identify the wake boundaries. These information are important to investigate the pitch up phenomenon and give experimental reference for numerical code evaluation and comparison. In figure 8 and 9, the horizontal and vertical mean velocities are reported. These values are obtained by averaging the time history in each point for all the time interval. The figures regard the transverse in the zone of tail #2 on the left side of the helicopter, for advance ratios of 0.015, 0.02 and 0.03. The graphs show that the tail in position #2 is affected by the rotor wake inducing the pitch-up phenomenon

on the helicopter. Moreover, the rotor wake moves backwards for increasing advance ratios.

The figures 10 and 11, regard the transverse in the zone of tail #3 on the left side of the helicopter, for advance ratios of 0.03, 0.04 and 0.05. The graphs show that the tail in position #3 is affected by the rotor wake especially for advance ratios of 0.05 inducing the pitch-up phenomenon on the helicopter. For advance ratio of 0.04 the influence is of lower intensity while for advance ratio of 0.03 it seems that the tail #3 is not affected by the rotor wake at all. Moreover, there is a sensible withdrawal at increasing advance ratios. The figures 12 and 13 regard the velocity behavior in the zone of tail #2 on the right side of the helicopter, for advance ratios of 0.015, 0.02 and 0.03. The rotor wake has a sensible withdrawal for increasing advance ratios. Therefore the tail in position #2 is affected by high vertical velocities for advance ratios of 0.02 and 0.03. In figure 14 and 15, a comparison of the rotor wake behaviour in the left and right side are reported. The graphs shows that both sides of the rotor wake are sensible to the variation of the advance ratio, resulting in the withdrawal of the wake at increasing advance ratios. The velocities are more intense in the right side (advancing side). This phenomenon is more evident for U components. This is due to the presence of the fuselage. Anyway W component converge to 35 m/s under the rotor wake for both sides and all advance ratio values.

7.2. Rotation-Averaged Velocity Field

The time history is splitted in each rotation and they all have been averaged to extract the behaviour of the flow within a complete rotation. In this way the quantities not in phase are eliminated and the periodic characteristics can be evaluated. The graphs reported in this section regard the transverse for the TP #3, left side at μ=0.05 (Fig. 16). The others conditions are similar and will not reported. The flow behaviour depends by the zone of investigation respect to the wake position. Three points have been selected to highlight the three different zones. The A point located at x=0.3m represents the zone far from the rotor wake: the influence of the blades induced velocities are clear visible. The diagram shows differences in magnitudes with a periodicity of 180° (Fig. 17). The B point located at x=0.18m represents the zone under the shear layer: the influence of tip vortices in the shear layer is manifest (Fig. 18). The C point located at x=0.02m represents the zone under the rotor wake. The velocities are the result of the induced velocities by big tip vortices and by the layer of the small vortices that leaves the blade along the span (Fig. 19).

7.3. Frequency Analysis

The frequency content of the wake was determined using Fast Fourier Transforms on the velocity time histories to obtained power spectral density. The examination of the FFT reveals, not unexpectedly, that essentially all of the energy in the wake spectrum is concentrated in frequencies which are multiples of the rotor frequency. The graphs reported in this section regard the transverse in tail plane position #3, left side, at advance ratio of 0.05. The other conditions are similar and so are not reported. As showed in the previous sections the velocity field near the rotor wake can be divided in three regions, one far from the rotor wake, one under the rotor wake and a transition zone. In this section the FFT of the same three points, analysed in the previous section and named A, B, C will be evaluated and reported.

In the figure 20, the FFT for the point A is reported. This point is representative of the region far from the rotor wake. The main contributes are due to the blade passages. In fact there are peaks at 24, 47 and 95 Hz.

A similar behaviour can be seen in the figure 21 that regards the FFT for the point B. This point is representative of the region at the boundary of the rotor wake and it is characterised by big tip vortex. The main contributes are due to the blade passages. In fact there are peak at 24, 47 and 95 Hz. Actually there are also high peaks at frequencies 140 and 190 that are 6 and 8 time the blade frequency, respectively. This means that there are phenomenon associated at the blade passage, for example from figure 18 it is possible to note that there is an instability at high frequency inside the passage of big vortices and this can cause the mentioned peaks.

The figure 22 regards the FFT for the point C. This point is representative of the region under the rotor wake. The main contributes are due to the blade passages. In fact there are peak at 24, 47 and 95 Hz.

In all points the highest peaks are at 47 and 95 Hz pointing out the phenomenon already seen previously. The rotor blades do not induce velocities with a 360° periodicity but there a remarkable contribution at 180°.

8. Glue On Probes Results

The aim of this section is to describe the results of the tests performed with the Glue On probes on the left tail plain (Position 2) and on the fuselage. The first set of 4 glue on probes have been stuck on the fuselage as in the following: the #1 in proximity of the leading edge of the tail plane #2 (-1cm from the reference), the #4 in proximity of the leading edge of the tail plane #3 (20 cm from the reference), and remaining two equidistant between ¼ cord (15 cm) of the tailplane #2 and the

leading edge of the tail plane #3 [15]. So the glue on probe #2 is located at 9 cm from the reference and #3 is located at 14.5 cm from the reference (fig. 23).

The second set of 4 glue on probes have been stuck on the tail plane in position #2, two on the upper and two on the lower side of the tail plane along the outboard pressure transducer line, at 5 and 10 cm from the leading edge.

8.1. Rotation-Averaged Velocity Field

The figure 24 regards the rotation average time history of the sensor#1 on the TP #2 for μ=0.04. This is an example where the flow is attached and it is possible to note the passage of the blades. In the figure 25 the flow is separated, the averaged voltage is lower than the null voltage, this is due to the effect of temperature drift. The other rotation-averaged graphs are quite similar so it will not reported.

A set of 4 glue-on probes were mounted on the fuselage and another one on the TP. Two configuration were performed, with and without the TP. The status of the flow on the TP (in the point of measurement) was "attached" for the sensor #1,2,3 for all advance ratio. The status of the flow for the sensor #4 is "attached" for μ = 0.015 while is separated for the other advance ratio.

The status of the flow on the fuselage without TP is attached for all the sensors for all advance ratio.

The status of the flow on the fuselage with the TP is attached for all sensors for all advance ratio except for sensor #4 at μ= 0.05.

9. PIV measurements main results

PIV measurements have been performed in correspondence of the second and third tail plane positions. The particle position has been captured by the digital camera at two sequential time instant. A measured zone of 180.6x144.5 mm^2 has been recorded.

"Fig. 26" presents the instantaneous velocity field for position 2 of the TP at 0.03 advance ratio. The velocity vector plot clearly shows the flow structures of the flow. The main rotor wake is clearly detectable on the left side while in the shear layer zone a strong tip vortex is present. The condition presented in the above mentioned figures is the typical pitch-up phenomenon, when the blade tip vortex impact to the tail position providing a high instability to the helicopter maneuverability. The vortex impacting on the tail plane provide an high concentration of energy to the airframe inducing also vibration besides to the increasing of the loads and the change of the pitching moment due to the wake.

To produce a time averaged velocity map it is necessary: to record a sufficient number of double-images of this type, to process each double image, so as to produce an instantaneous velocity map and to compute the average and in some cases the standard deviation of the instantaneous velocities. In the case of these measurements, 50 double images were recorded for each test section. This number is certainly too low to produce a reliable time average velocity map. However the main aim of this campaign was to check the feasibility of these measurements, and to explore the potential of the technique in some area of interest of rotorcraft flow investigation.

Fig. 27 presents the time average velocity field obtained on 50 instantaneous velocity maps together with the colour map of the module of the velocity. In this way the velocity gradient long the x direction is clearly detected. The results of the PIV measurements are reported elsewhere [20, 25].

10. HW and PIV measurements comparison

In this section, the most interesting comparisons between HW and PIV measurements are reported. The comparison regards the time averaged velocities, the locating of the PIV survey regarding the azimuth angle and the position of the wake boundary.

10.1. Time averaged comparison

Within part of the HWA traverse range there was also the possibility to extract the velocity components from a corresponding section across the PIV images. These mean velocity component profiles are compared in figures 28 and 29 for an advance ratio 0.03. Using data from a full complement of zones and tailplane locations, these plots include four sets of velocities derived from PIV and two sets for HWA. It is seen that the vertical velocities, for each technique, are closely self-consistent but there is a difference between the PIV and HWA, corresponding to a horizontal shift of wake location of about 0.05m. For all the cases, the vertical velocities measured with HW system are constantly higher than PIV one.

The following reason can be illustrated:

- Systematic error of each measurements technique;
- Interference of the traversing system on HW measurements;
- Influence of V_y (out of measurement plane component) on PIV and HWA measurements;

- The PIV samples are not enough to evaluate an accurate velocity ensemble average value.

The horizontal velocity shows a better agreement. The differences are more evident under the rotor wake [24].

10.2. PIV azimuth angle locating

Another interesting comparison has been performed between the data acquired with PIV and HWA.

The HWA data are synchronized with the passage of the blade and so in each point it is possible to know the velocity components as functions of the blade position. These velocity components are the results of the averaged velocities on 23 rotations. The angle resolution is about 0.3° having about 1200 samples per rotation.

For some test conditions the PIV system was phase locked to the helicopter main rotor without being synchronised. Conditional ensemble velocity field has been obtained without knowing the corresponding azimuth angle position.

For the μ= 0.03, 0.04 and 0.05 a comparison between PIV and HWA data have been performed in order to detect the azimuth angle correspondent to the PIV phase locked acquisition. For this kind of investigation it has been necessary to compare the PIV velocity components with the 1200 angles provided by HW. PIV data have been interpolated to extract the points corresponding to HWA acquisition.

The difference between the PIV and the HWA data has been calculated for each available azimuth angle. The corresponding PIV angle position has been obtained find out the minimum value of the data difference, i.e. the angle position that PIV data better match the HWA data. An example of the result of this comparison are reported in the figures 30 and 31.

10.3. Wake boundary locating

The analysis of the time averaged velocities gives the indication of the skew angle of the rotor wake and its position relative to the reference system. These information can be deducted from the figures 8 – 13 for HW, while the PIV ones are reported in [24, 25].

For μ = 0.015, the data locates the boundary of the rotor wake approximately at –11cm up stream the leading edge of tail plane n° 2, while the shear layer ends at +2 cm down stream the leading edge of the tail plane n° 2.

For μ = 0.02, the data locates the boundary of the rotor wake approximately at –9 cm up stream the leading edge of tail plane n° 2, while the shear layer ends at +10 cm down stream the leading edge of the tail plane n° 2.

For μ = 0.03, the data locates the boundary of the rotor wake approximately at –4 cm up stream the leading edge of tail plane position n° 2, while the shear layer ends at +17 cm down stream the leading edge of the tail plane position n° 2.

For μ = 0.04, the data locates the boundary of the rotor wake approximately at 8 cm down stream the leading edge of tail plane position n° 2, while the shear layer ends at +20 cm down stream.

For μ = 0.05, the data locates the boundary of the rotor wake approximately at +15 cm down stream the leading edge of tail plane position n° 2, while the shear layer ends at +25 cm down stream.

The different rotor wake location by HWA and PIV data have been carefully investigated in order to give a reasonable interpretation. The different location of the wake, obtained by the two different measurements systems, could be due to the interference provided by the traversing and support system utilised with the HW probe and not used during the PIV tests.

The location of the wake obtained by HWA and PIV at -20 m/s illustrates quite constant shift (fig. 32). The shift is about 5 cm. Subtracting the shift value at 0.03 advance ratio, the trend of the wake positions well fitted (fig. 33).

11. Conclusions

The main scope of this experimental campaign “to demonstrate the applicability of the Particle Image Velocimetry and Hot Wire at industrial wind tunnel, investigating highly unsteady phenomena”, has been fully fulfilled.

At 24 ft wind tunnel, the PIV and HW measurements have been performed investigating the behaviour of the flow field during the pitch up condition. Different aspects regarding the integration of the PIV system with the wind tunnel have been investigated and solved thanks to a close and fruitful collaboration with the colleagues of DERA.

The investigation of the flow conditions resulting from the changes of aircraft pitching moment associated with the main rotor wake impinging on the rear of the fuselage and tailplanes have been fulfilled.

The comparison of the ensemble average velocity fields has been evaluated, the behaviour of the x and z components of the velocity, along the X axes, have been illustrated in this report.

The position of the vortex trajectories has been individuated and the critical condition of the pitch phenomena has been verified.

The pitch up condition, individuated by the lift measurements performed by the tail plane balance, for the position 2 has been verified and demonstrated correct whereas the condition and the values of the advance ratio reported by the balance for the position 3 were not accurate. In fact for the values of 0.03, 0.04 and 0.05 of advance ratio the shear layer still impact to the position 2 of the tail plane. For μ=0.05, the shear layer slightly influences the tail plane. The flow measurements do not take into account the influence on the flow pattern performed by the tail plane that in our case were removed.

An accurate velocity measurements have been provided in order to validate numerical code [26].

Acknowledgement

This work has been performed in the framework of the Brite Euram III project BPR CT 96-0206 HELIFLOW. The authors wish to acknowledge the valuable contributions enabling the success of this investigation by the DERA 24 feet WT team, for the support given during the measurement, and in particularly Dr. R.H. Markiewicz and Mr. K.Thornton. Mr. I. Kaynes for the co-ordination of the task 1 and 2 of the Heliflow project and Dr. G. Preatoni for his friendship and the useful contribution in designing the helicopter fuselage and providing his experience in the aerodynamics of the helicopter.

References

1 Rabbott Jr., J. P., "Static-thrust Measurements of the Aerodynamic Loading on a Helicopter Rotor Blade," NACA TN 3688, Langley Aeronautical Laboratory, National Advisory Committee for Aeronautics, Langley Field, Virginia 1956

2 Gray, R. B., and McMahon, H. M., and Shenoy, K. R., and Hammer, M.L., " Surface Pressure Measurements at Two Tips of a Model Helicopter Rotor in Hover," NASA CP-3281, May 1980

3 Kocurek, J.D., and Tangler, J. L., " A Prescribed Wake Lifting Surface Hover Performance Analysis," 32ndAnnual National Forum of the American Helicopter Society, Preprint No. 1001 May 1976

4 FAA Technical Center," Helicopter Full Scale Wake Flight Research," FAA Technical Center TV Facility Video TST 179.16, November 1987

5 Muller, R. H. G., " Helicopter Rotor Wake Visualisation in Forward Flight," 8th Int. Symp. On Flow Visualisation, 69, Sorrento (Italy) 1998

6 Sullivan, J. P., "Experimental Investigation of Vortex Rings and Helicopter Rotor Wakes Using a Laser Doppler Velocimeter," D. S. Dissertation, Massachussetts Institute of Technology, 1973

7 Leishman J.G. Baker A. Coyne A. "Measurements of Rotor Tip Vortices using three-component Laser Doppler Velocimetry", Journal of American Helicopter Society, pp342-353, October, 1996.

8 Landgrebe, A. J., and Johnson, B.V., "Measurements Of Model Helicopter Rotor Flow Velocities with a Laser Doppler Velocimeter," Tech. Note, J. Am. Helicopter Soc. 19, No.2 1974

9 Cook, C. V., " The Structure of the Rotor Blade Tip Vortex," Westland Helicopters, Research Paper No. 430, 1972

10 Caradonna, F. X., and Tung, C., "Experimental and Analytical Studies of a Model Helicopter Rotor in Hover," Vertica vol.5 1981

11 Cheeseman, I. C., and Haddow, C., "An Experimental Investigation of the Downwash Beneath a Lifting Rotor and Low Advance Ratios," 14th European Rotorcraft Forum, Paper No. 8, Milano September 1988

12 Moedersheim, E., and Leishman, J. G., ".Investigation of Aerodynamic Interactions between a Rotor and a T-Tail Empennage," 22nd ERF, 1995.

13 Prouty, R. W., "Development of the Empennage Configuration of YAH-64 Advanced Attach Helicopters," USAAVRADCOM-TR82-D-22, Feb. 1983.

14 R H Markiewicz ,"Description of the wind tunnel tests for task1 and 2 of the CEC Heliflow program,"DERA/MSS/MSTR2/CR990069 May 1999.

15 Tino, N., " Heliflow - Task 1-Results of the Hot Wire Measurements of the 24ft Dera Wind Tunnel Tests," CIRA-TR-LAS-99-086

16 I W Kaynes ,R H Markiewicz ,K R A Thornton, "Description of the DRA Rotor Rig and the 24ft Wind Tunnel for Heliflow," DERA/ASD/CR96353, DERA, November 1996.

17 R H Markiewicz ,"Detailed Description of the DERA Rotor Rig Hub and the PM1 Rotor Blades for Heliflow," DERA/MSS5/CR980170/1.0, DERA, 1998.

18 S.P. Parthasarathy, D.J. Tritton "Impossibility Of Linearizing Hot-Wire Anemometer For Turbulent Flows" AIAA Journal Vol.1, 1963.

19 H. H. Bruun "Hot Wire Anemometry – Principles and Signal Analysis" Oxford Science Publications.

20 Barbagallo, D., De Gregorio, F., Tino, N., " Helicopter Wake Investigation by Means of PIV and HW Measurement Techniques,". 9th ISFV, Edimburg, Sept. 2000.

21 Willert C, The fully digital evaluation of photographic PIV recordings. Appl. Scientific Res. 59 79-102, 1996.

22 Guj G., Terzitta M. and Suffi G. " Velocity measurement upstream of a windmil rotor model" Wind Eng. 15,5-(1991).

23 F. E. Jorgensen. "Directional sensitivity of wire and fiber films probes." DISA Inf. Dept. 11,31, 1971.

24 F. De Gregorio, N Tino, HELIFLOW HW and PIV results comparison. CIRA-TR-LAS-99-211, CIRA, February 2000.

25 F. De Gregorio, Heliflow Pitch-Up phenomenon characterisation by PIV. CIRA-TR-LAS-99-098, CIRA, May 1999.

26 F.Tchen-Fo,C.Allain,A.Desopper Improved vortex ring model for helicopter pitch up prediction, 26th ERF,The Hague, NL, September 2000.

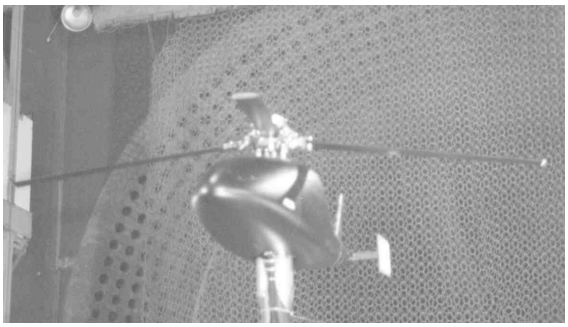

Fig. 1: AGUSTA Helicopter model

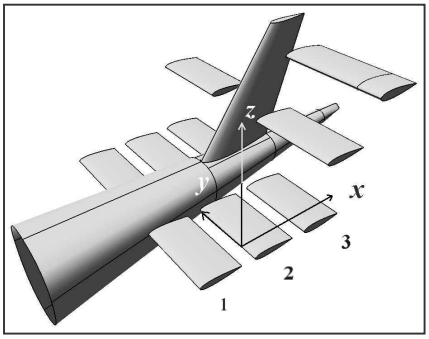

Fig. 2: Tail plane position and Ref. Sys.

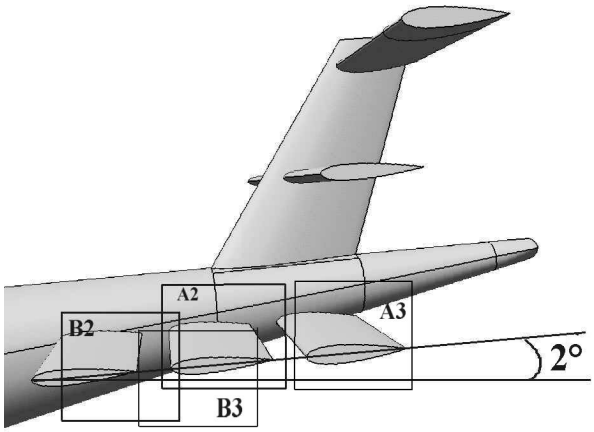

Fig. 3: PIV measured areas

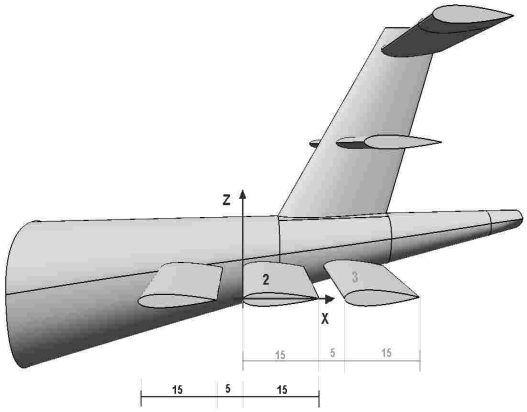

Fig. 4: HW Investigated axes

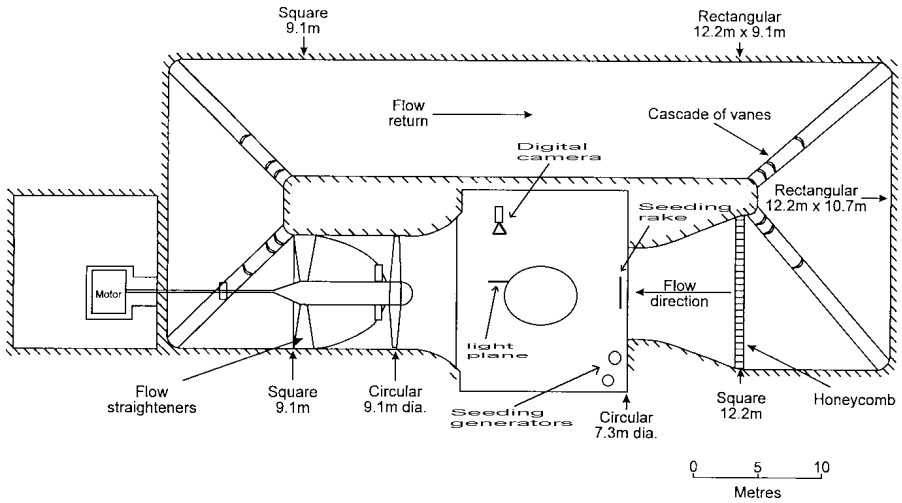

Fig. 5: Wind tunnel layout

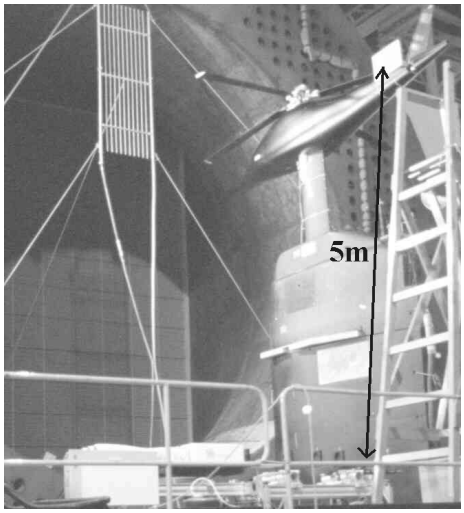

Fig. 6: Wind tunnel test chamber

Fig. 7: HW probe support mounted on traversing pylon

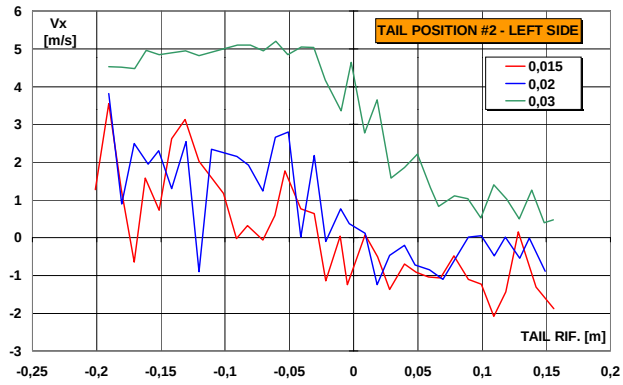

Fig. 8: Time Averaged horizontal velocity

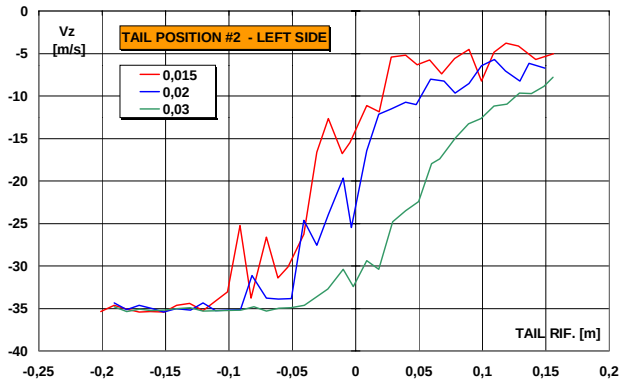

Fig. 9: Time Averaged vertical velocity

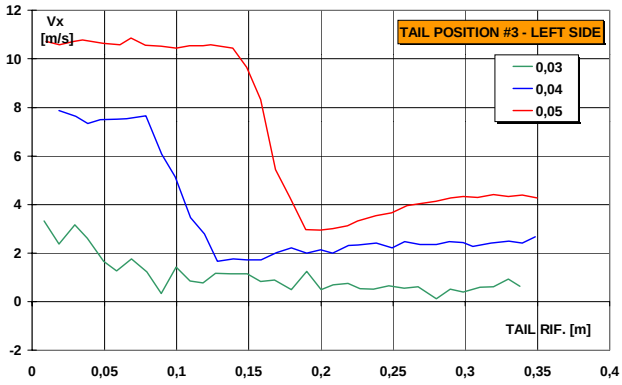

Fig. 10: Time Averaged horizontal velocity

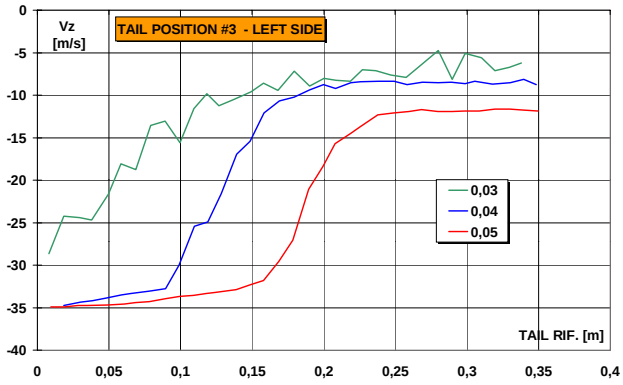

Fig. 11: Time Averaged vertical velocity

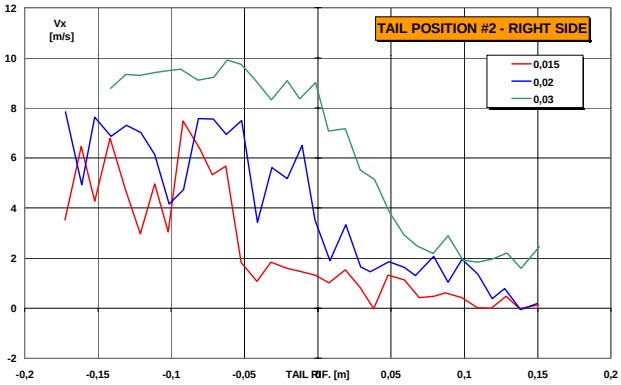

Fig. 12: Time Averaged horizontal velocity

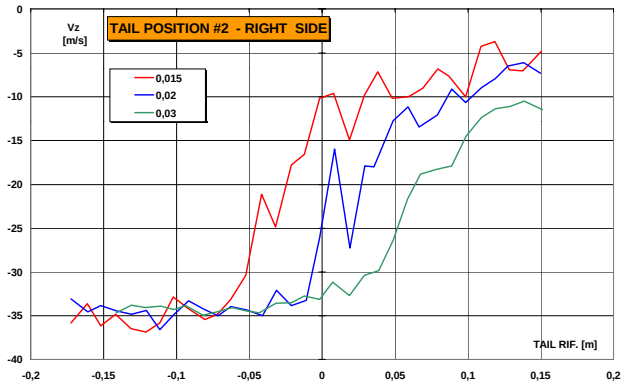

Fig. 13: Time Averaged vertical velocity

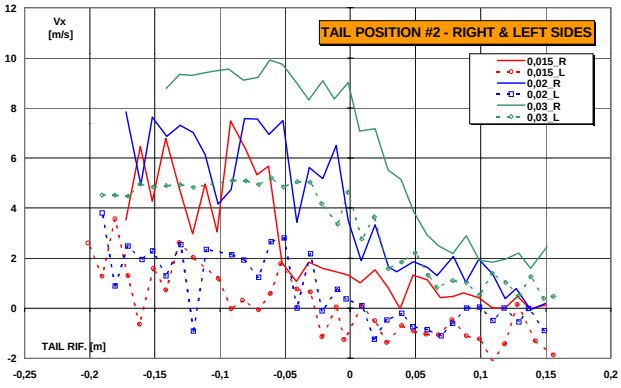

Fig. 14: Comparison of averaged horizontal velocity

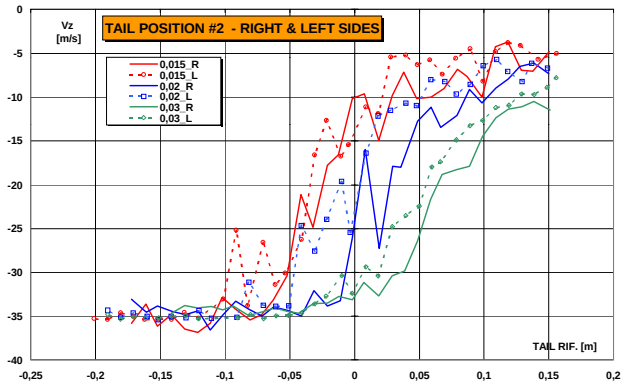

Fig. 15: Comparison of averaged vertical velocity

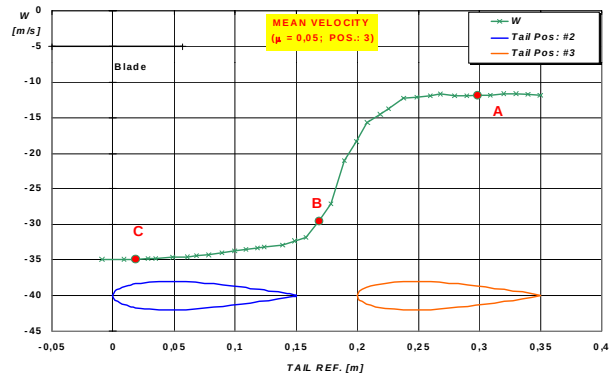

Fig. 16: Time Averaged vertical velocity

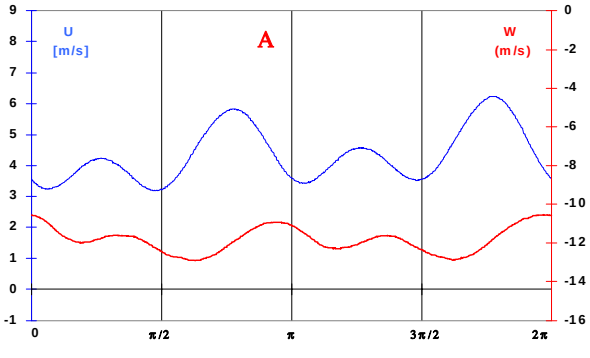

Fig. 17: Rotation averaged velocities (A, x=0.3m)

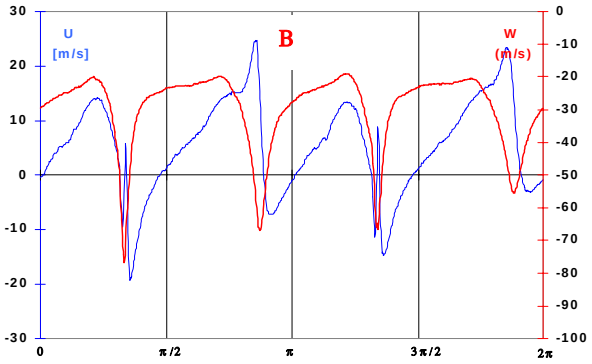

Fig. 18: Rotation averaged velocities (B, x=0.18m)

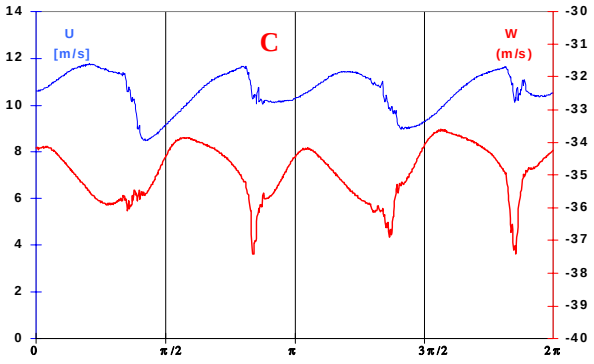

Fig. 19: Rotation averaged velocities (C, x=0.02m)

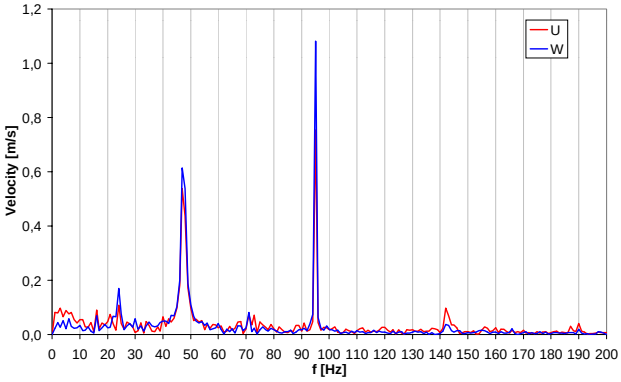

Fig. 20: FFT at position A, x=0.3m

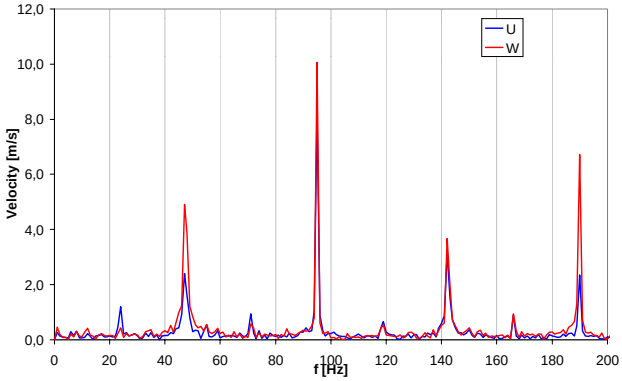

Fig. 21: FFT at position B, x= 0.18m

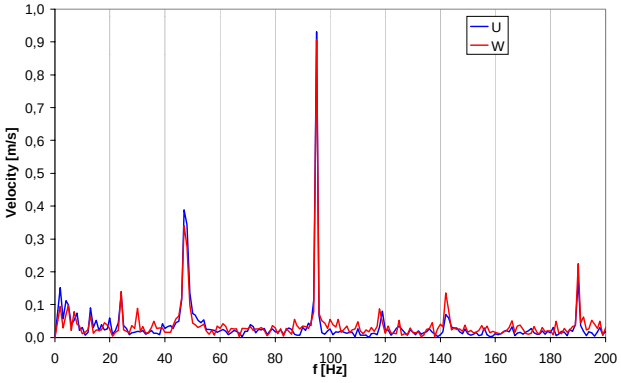

Fig. 22: FFT at position C, x= 0.02m

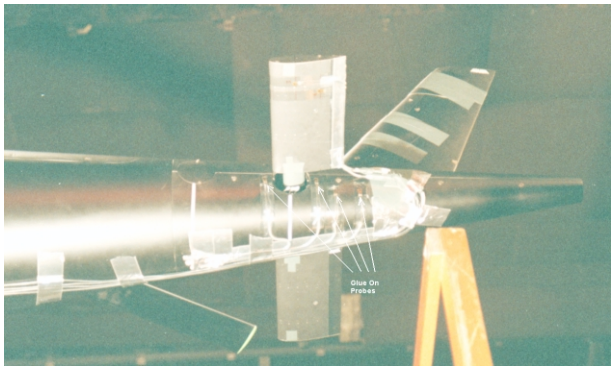

Fig. 23: Investigated Areas with Glue-on Probes

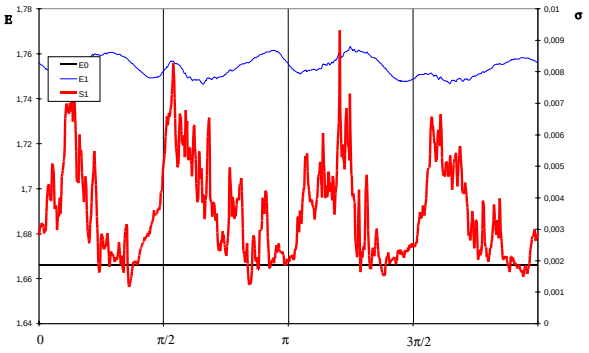

Fig. 24: Rotation-Averaged Voltage and STD Dev.

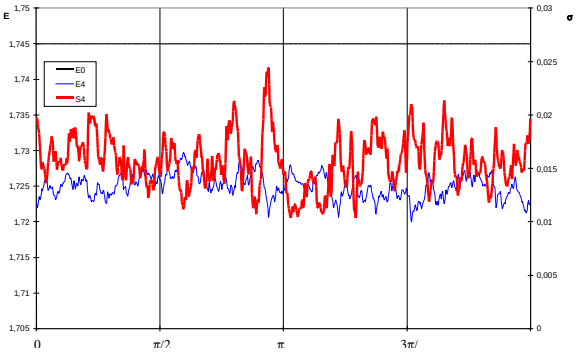

Fig. 25: Rotation-Averaged Voltage and STD Dev.

Instantaneous Velocity Field (PIV)

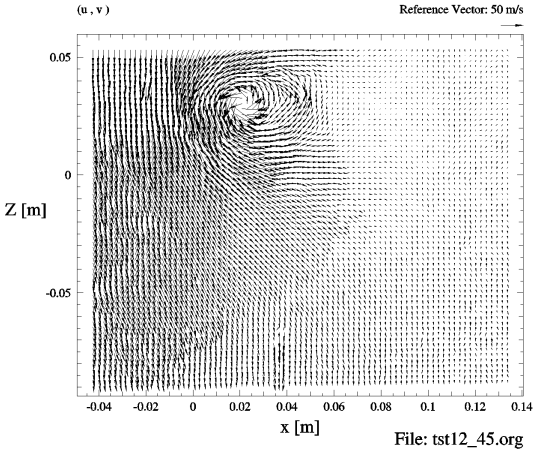

Fig. 26: Instantaneous Velocity Field

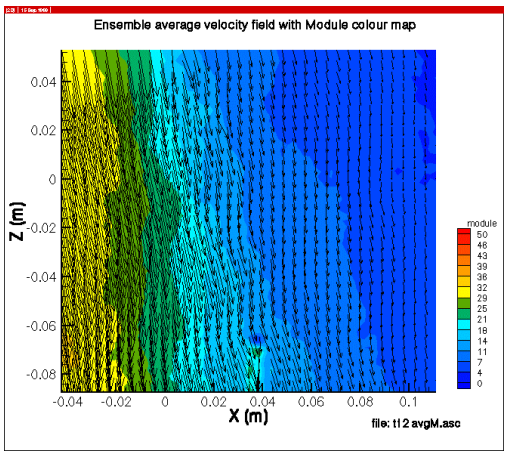

Fig. 27: Ensemble Average Velocity Module

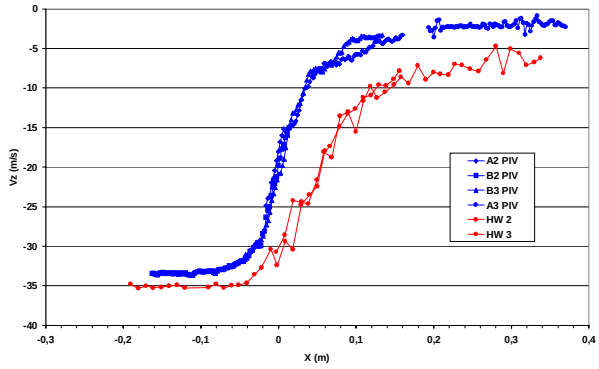

Fig. 28: Hot Wire and PIV Results Comparison (Vz)

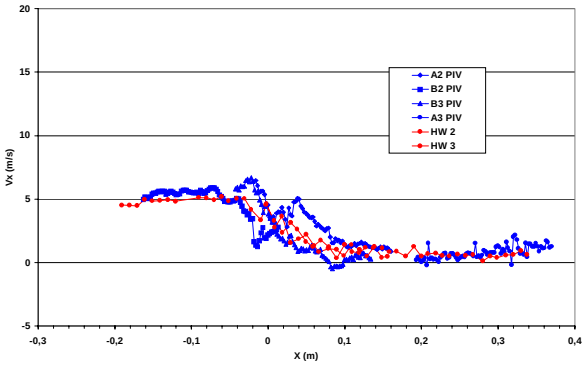

Fig. 29: Hot Wire and PIV Results Comparison (Vx)

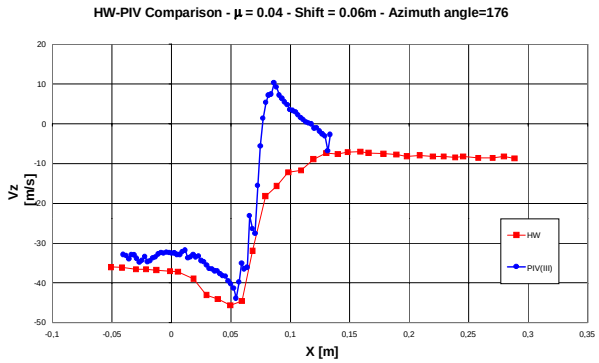

Fig. 30: PIV Azimuth Angle Locating (Vz)

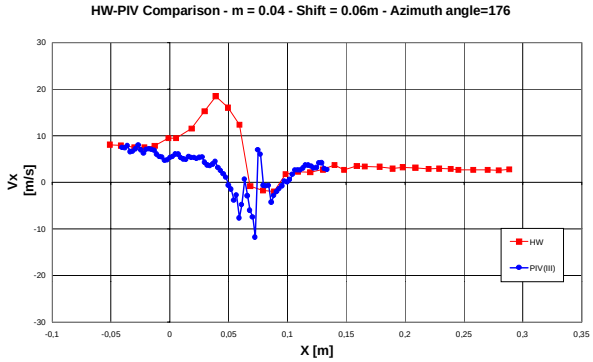

Fig. 31: PIV Azimuth Angle Locating (Vx)

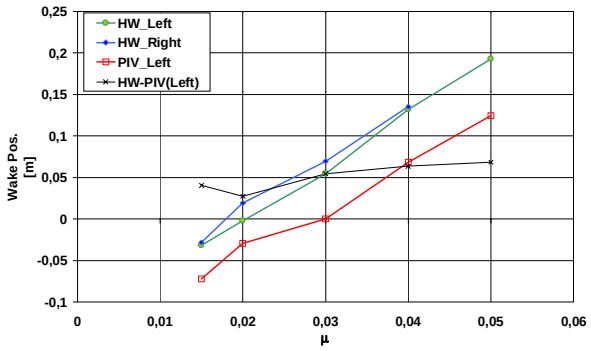

Fig. 32: Wake Position at 20 m/sec

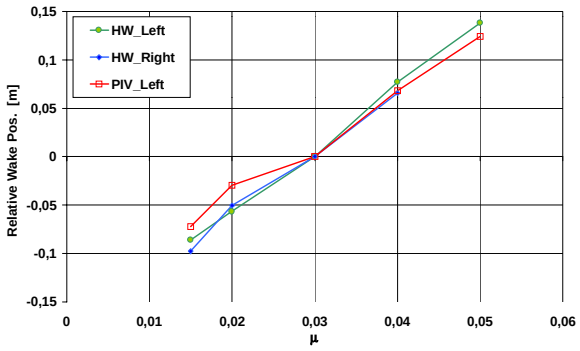

Fig. 33: Relative Wake Position at 20 m/sec